Interannual-to-Decadal Variability in the Bifurcation of the North Equatorial Current off the Philippines

BO QIU AND SHUIMING CHEN

Department of Oceanography, University of Hawaii at Manoa, Honolulu, Hawaii

(Manuscript received 8 March 2010, in final form 16 June 2010)

ABSTRACT

Satellite altimeter sea surface height (SSH) data from the past 17 yr are used to investigate the interannual-to-decadal changes in the bifurcation of the North Equatorial Current (NEC) along the Philippine coast. The NEC bifurcation latitude migrated quasi decadally between 10° and 15°N with northerly bifurcations observed in late 1992, 1997–98, and 2003–04 and southerly bifurcations in 1999–2000 and 2008–09. The observed NEC bifurcation latitude can be approximated well by the SSH anomalies in the 12°–14°N and 127°–130°E box east of the mean NEC bifurcation point. Using a 1 ½-layer reduced-gravity model forced by the ECMWF reanalysis wind stress data, the authors find that the SSH anomalies in this box can be simulated favorably to serve as a proxy for the observed NEC bifurcation. With the availability of the long-term reanalysis wind stress data, this helps to lengthen the NEC bifurcation time series back to 1962. Although quasi-decadal variability was prominent in the last two decades, the NEC bifurcation was dominated by changes with a 3–5-yr period during the 1980s and had low variance prior to the 1970s. These interdecadal modulations in the characteristics of the NEC bifurcation reflect similar interdecadal modulations in the wind forcing field over the western tropical North Pacific Ocean. Although the NEC bifurcation on interannual and longer time scales is generally related to the Niño-3.4 index with a positive (negative) index corresponding to a northerly (southerly) bifurcation, the exact location of bifurcation is determined by wind forcing in the 12°–14°N band that contains variability not fully representable by the Niño-3.4 index.

1. Introduction

The North Equatorial Current (NEC) is a westward confluent current of the interior Sverdrup flows of the North Pacific subtropical and tropical gyres. After encountering the western boundary along the Philippine coast, the NEC bifurcates into the southward-flowing Mindanao Current (MC) and the northward-flowing Kuroshio (e.g., Nitani 1972; Toole et al. 1990; Hu and Cui 1991). At the crossroads of the subtropical and tropical circulations, the bifurcating NEC provides important pathways for heat and water mass exchanges between the mid- and low-latitude North Pacific Ocean (Fine et al. 1994; Lukas et al. 1991). Because the western Pacific warm pool with sea surface temperatures >28°C extends poleward of 17°N (Locarnini et al. 2006), the NEC's bifurcation and transport partitioning into the Kuroshio and MC are likely to affect the temporal evolution of the warm pool through lateral advection. In addition to its influence on physical conditions, changes in the NEC bifurcation are also important to the regional biological properties and fishery variability along the Philippine coast and in the western Pacific Ocean (e.g., Amedo et al. 2002; Kimura et al. 2001).

Located at the western boundary of the Pacific basin, the NEC bifurcation is subject to both the local monsoonal wind forcing and the remote forcing of the broad-scale interior ocean via baroclinic Rossby waves (Qiu and Lukas 1996). On the seasonal time scale, analyses based on historical hydrographic data, assimilation model output, and satellite altimeter measurements reveal that the bifurcation latitude reaches its northernmost position in November/December and its southernmost in May–July (Qu and Lukas 2003; Yaremchuk and Qu 2004; Wang and Hu 2006). This seasonal migration of the NEC bifurcation agrees in general with the predictions based on a 1 ½-layer reduced-gravity ocean model (Fig. 9 in Qiu and Lukas 1996) and a full-fledged ocean general circulation model (Fig. 4 in Kim et al. 2004). Both models find a southernmost NEC bifurcation in April/May, with its northernmost counterpart in October/November.

Corresponding author address: Dr. Bo Qiu, Department of Oceanography, University of Hawaii at Manoa, 1000 Pope Road, Honolulu, HI 96822.
E-mail: bo@soest.hawaii.edu

DOI: 10.1175/2010JPO4462.1

© 2010 American Meteorological Society

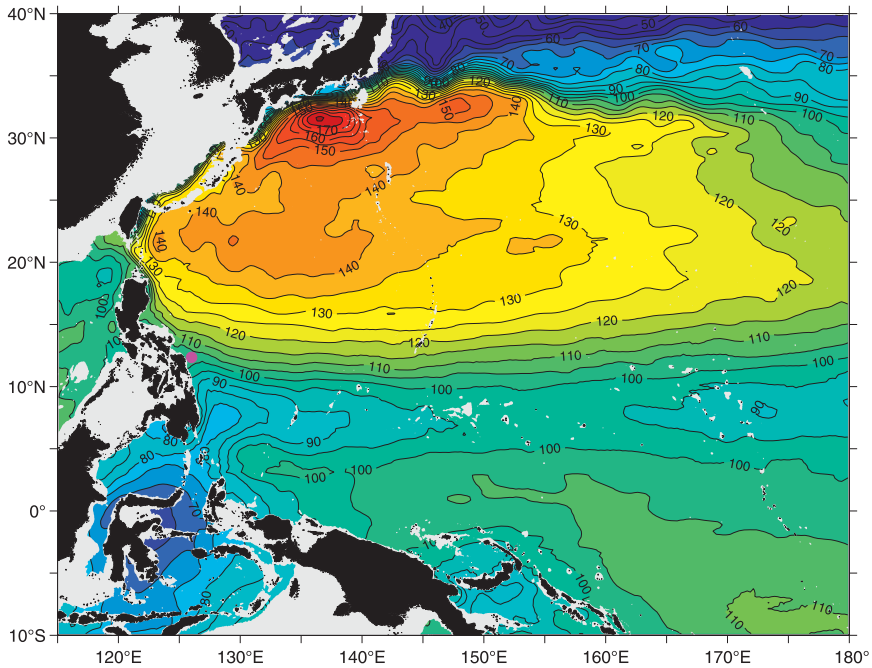

FIG. 1. Mean sea surface height field (cm) of the western Pacific Ocean from Rio et al. (2009). Gray shadings denote areas where water depth is shallower than 1000 m. Pink dot near 12°N along the Philippine coast indicates the location of the mean NEC bifurcation.

One consistent feature of both the data analyses and numerical models is that the annual excursion of the NEC bifurcation is about 2° latitude, much smaller than the 10° annual excursion of the zero wind stress curl line averaged across the Pacific basin. Dynamically, it takes baroclinic Rossby waves ~(2.5–3) yr to traverse the Pacific basin in the 10°–15°N band of the bifurcating NEC. Effects of the annually forced baroclinic Rossby waves tend to cancel out destructively following the wave paths, resulting in a much reduced seasonal migration of the NEC along the western boundary (Qiu and Lukas 1996). The monsoonal wind forcing near the Philippine coast, on the other hand, exerts a larger impact on the seasonal NEC bifurcation because it experiences no along-path destructive cancellations.

For the wind forcing with interannual and longer time scales, the along-path cancellation effect also becomes less significant because the same-signed baroclinic Rossby waves are induced across the Pacific basin. Compared to the seasonal signals, our knowledge of the lower-frequency changes in the NEC bifurcation is limited by a lack of systematic measurements. Though sporadic, large interannual changes in the NEC bifurcation have been detected in in situ observations. For example, Toole et al. (1990) observed a twofold increase in transport values of the NEC, the MC, and the Kuroshio in spring 1988 as compared with autumn 1987. Accompanying the transport increase was a northward migration of the NEC bifurcation from 12.6° to 14.1°N. Similar large transport changes in the NEC and the MC were also detected more recently by Kashino et al. (2009) in their December 2006 and January 2008 cruises off the Philippine coast. They attributed the observed increased transport in December 2006 to the warm phase of the El Niño–Southern Oscillation (ENSO) phenomenon. The change in bifurcation latitude is not obvious from their hydrographic surveys of the NEC along 130°E (their Fig. 3).

Accumulation of high-quality sea surface height (SSH) data from satellite altimeters over the past 17 yr provides us now with an effective means to explore interannual-to-decadal changes in the surface ocean circulation. As the bifurcating NEC and the originating MC and Kuroshio all have large cross-stream differential SSH signals (see Fig. 1), satellite altimeter measurements are well suited to detect their variability in a systematic way. The present study has three objectives. The first is to describe the time-varying NEC bifurcation along the Philippine coast based on the 17-yr satellite altimeter data. Well-defined, quasi-decadal changes with a peak-to-peak amplitude exceeding 5° latitude are detected. The second objective is to examine the dynamics underlying the observed bifurcation changes. This is pursued by adopting a 1 ½-layer reduced-gravity model forced by reanalysis surface wind stresses. Our third objective is to extend the time series of the NEC bifurcation back in time with the use of the dynamic model and proxy regional SSH anomaly

data. With the long time series from 1962, we attempt to clarify the degree to which the interannual-to-decadal variability in the NEC bifurcation can be attributed to the ENSO-related wind stress curl forcing.

2. Identification of the NEC bifurcation from satellite altimetry

To examine the NEC's bifurcation along the Philippine coast, we use the global SSH anomaly dataset compiled by the Collocte Localisation Satellites (CLS) Space Oceanographic Division of Toulouse, France. The dataset merges the Ocean Topography Experiment (TOPEX)/Poseidon, *European Remote Sensing Satellite-1* (*ERS-1*) and *ERS-2*, *Geosat Follow-On*, and *Jason-1* and *Jason-2* along-track SSH measurements (Le Traon et al. 1998; Ducet et al. 2000). It has a $1/3° \times 1/3°$ Mercator spatial resolution and covers the period from October 1992 through December 2009. Because the focus of the present study is on the low-frequency NEC bifurcation, the original weekly dataset is temporally averaged to form the monthly SSH anomaly dataset.

For identification of the NEC bifurcation, information about the mean SSH field is required. In this study, we adopt the hybrid mean dynamic topography produced by Rio et al. (2009). This mean SSH field, known as MDT_CNES-CLS09, combines the GRACE geoid, surface-drifter velocities, profiling float, and hydrographic temperature–salinity data. It has a $1/4°$ spatial resolution. As shown in Fig. 1, this mean SSH field reveals that the NEC bifurcates at a mean latitude of ~12°N northeast of the island of Samar along the Philippine coast. This mean bifurcation latitude for the surface NEC agrees favorably with the values inferred previously based on historical hydrographic and surface drifter data (Nitani 1972; Centurioni et al. 2004; Yaremchuk and Qu 2004). For brevity, we will hereinafter refer to the NEC's bifurcation latitude as Y_b.

To determine the monthly $Y_b(t)$ values from the satellite altimeter data, we first calculate the meridional geostrophic velocity as a function of y along the Philippine coast,

$$v_g(y, t) = \frac{g}{f}[h_e(y, t) - h_w(y, t)], \qquad (1)$$

where h_w is the absolute (i.e., mean + anomalous) SSH value averaged in the 1° band east of the Philippine coast, h_e is the absolute SSH value averaged in the 1° band east of the h_w band, g is the gravity constant, and f is the Coriolis parameter. For each month, $Y_b(t)$ is obtained where $v_g(y, t) = 0$. In the case where multiple zero crossings are present along the Philippine coast, the $v_g(y, t) = 0$ point whose SSH value can be traced back (i.e., upstream) to the core of the westward-flowing NEC is selected. Figure 2a shows the time series of $Y_b(t)$ thus derived from October 1992 to December 2009. Because of the presence of the intraseasonal variability associated with the Mindanao Current (e.g., Qiu et al. 1999; Firing et al. 2005; Kashino et al. 2005), large month-to-month excursions are seen in the $Y_b(t)$ time series (gray line). Prevalence of the interannual-to-decadal variability in $Y_b(t)$ becomes easily discernible if a low-pass filter[1] is applied to the time series (solid line). As shown by the black line in Fig. 2a, the amplitude of the low-frequency Y_b variability is substantial and has a range from 9.5° to 15°N. Compared to this large migration on the interannual and longer time scales, the annual Y_b variation is small, with an amplitude of about 1° latitude: 11.5°–12.5°N (see Fig. 2b). In agreement with the previous studies reviewed in the introduction, the seasonal NEC bifurcation extends to its northernmost latitude around November–January and retreats to its southernmost latitude during April–July.

The altimeter-derived SSH data near coasts can possibly be affected by unremoved tidal signals (e.g., Le Provost 2001). To address this potential problem, a sensitivity analysis is conducted in which we used the SSH difference data 100 km offshore of the Philippine coast in Eq. (1). The resultant $Y_b(t)$ time series reveals a temporal pattern very similar to that of Fig. 2a, especially for the low-pass filtered signals (not shown). Because the observed SSH signals amplify toward the west, the bifurcation latitude based on the offshore SSH difference data tends to have a smaller (~94%) amplitude than that based on the near-shore SSH difference data. Given this sensitivity analysis, the $Y_b(t)$ time series in Fig. 2a can be regarded as a robust estimate representing the time-varying NEC bifurcation.

It is instructive here to relate the low-frequency Y_b signals to the broader-scale circulation changes in the western tropical Pacific Ocean. To do so, we compare in Fig. 3 the SSH field in four periods, during two of which (April 1997–March 1998 and January 2003–December 2004) the NEC had a northerly bifurcation and in the other two periods (January 1999–December 2000 and July 2007–June 2009) the NEC bifurcated at a southerly latitude. It is interesting to note that, when Y_b is southerly, the spatial circulation patterns shown in Figs. 3b,d are very similar. To a lesser degree, this is also true for the two circulation patterns when Y_b is northerly. Compared to the southerly bifurcation years, the tropical gyre, characterized by the SSH values lower than 105 cm,

[1] Throughout this study, low-pass filtering is done by applying a Gaussian filter with a form of $\exp(-d^2/2\sigma^2)$, where d is the temporal separation in months and $\sigma = 3.5$ months.

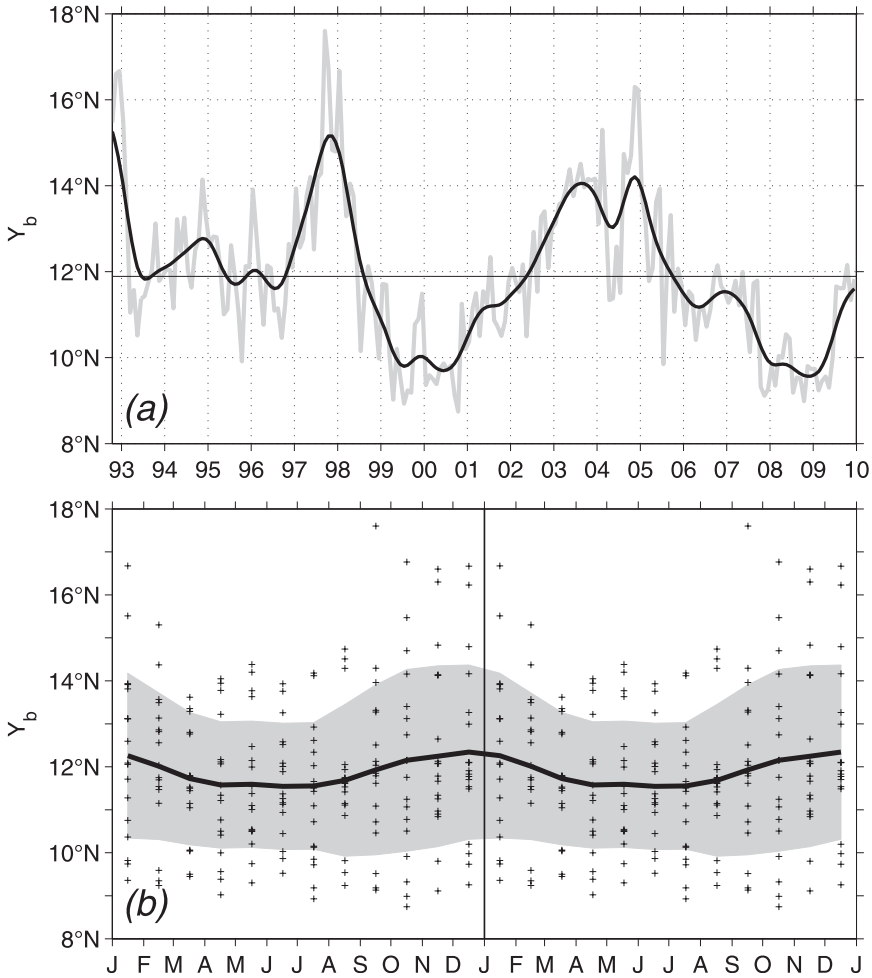

FIG. 2. (a) Time series of the NEC bifurcation latitude $Y_b(t)$ inferred from the monthly satellite altimeter SSH measurements (gray line). The black line indicates the low-pass filtered $Y_b(t)$ time series. (b) NEC bifurcation latitude as a function of calendar months. Here, pluses indicate individual Y_b estimates and the solid line (shaded band) denotes the monthly average (the standard deviation range).

has a better defined thermocline ridge along 7°–8°N in the northerly bifurcation years (Figs. 3a,c). Associated with the enhanced thermocline ridge, the intensity of both the NEC and the North Equatorial Countercurrent (NECC) is stronger in the northerly bifurcation years than in the southerly bifurcation years. Responding to the change in NEC's intensity, the strengths of the bifurcated Kuroshio and MC are also larger in the northerly bifurcation years. Notice that, as the NEC bifurcation shifts northward and the North Pacific tropical gyre intensifies, the SSH values in the Celebes Sea (approximately 1°–6°N, 118°–125°E), Sulu Sea (6°–12°N, 118°–123°E), South China Sea (8°–23°N, 115°–122°E), and Indonesian seas (5°S–1°N, 115°–132°E) also decrease.

Given the broad-scale SSH changes in connection with the $Y_b(t)$ signals, it is of interest to explore whether the SSH time series may be used as a proxy to represent the time-varying $Y_b(t)$ signals. Figure 4 shows the instantaneous correlation map between the monthly $Y_b(t)$ time series and the pointwise SSH time series in the western tropical Pacific Ocean. The highest correlation, $r \simeq -0.85$, is found at 13°N, 128°E, close to the mean location of the NEC bifurcation (recall Fig. 1). The correlation is negative near the mean bifurcation point because a northward (southward) shift in Y_b is connected to the expansion of the tropical (subtropical) gyre that has low (high) SSH values. With the high correlation value obtained locally near the mean bifurcation point, it is possible to construct through least squares fitting the following proxy bifurcation latitude $Y_p(t)$ using the observed SSH anomaly data there:

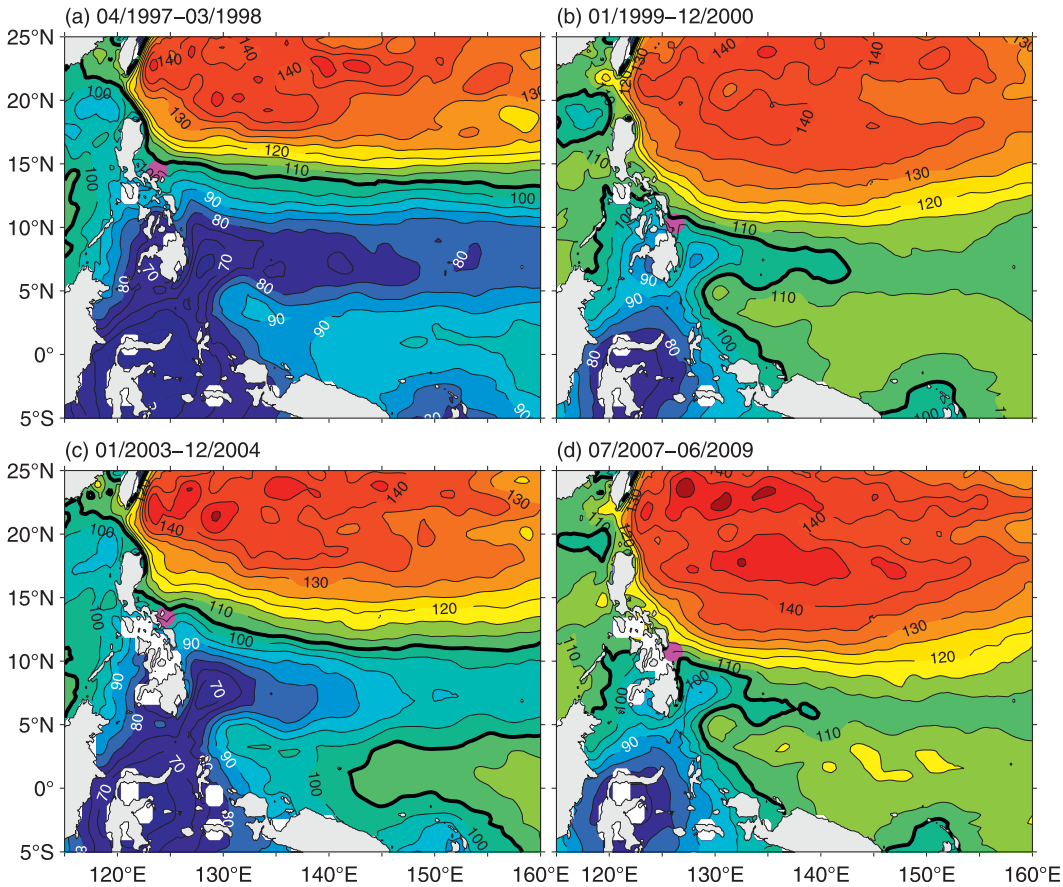

FIG. 3. SSH maps of the low-latitude western Pacific Ocean (cm) in (a) April 1997–March 1998, (b) January 1999–December 2000, (c) January 2003–December 2004, and (d) July 2007–June 2009. Pink dots denote the location of the NEC bifurcation. As indicated in Fig. 2a, the NEC bifurcates at northerly latitudes during periods in (a) and (c), and at southerly latitudes during periods in (b) and (d).

$$Y_p(t) = 11.9 - 0.13 \times h'(t) \quad (^\circ\mathrm{N}), \tag{2}$$

where $h'(t)$ is the monthly SSH anomaly value (in cm) averaged in the 12°–14°N and 127°–130°E box. The gray line in Fig. 5a shows the $Y_p(t)$ time series constructed according to Eq. (2). For the interannual-to-decadal signals of our interest (see the black solid and dashed lines in Fig. 5a), the predictive skill of $Y_p(t)$ to the observed NEC's bifurcation latitude reaches $S = 92.3\%$, where $S \equiv 1 - \langle (Y_p - Y_b)^2 \rangle / \langle (Y_b - 11.9)^2 \rangle$ and $\langle \cdot \rangle$ denotes the summation over time. Clearly, the SSH signals in the key region of 12°–14°N and 127°–130°E serve as an excellent proxy for the time-varying $Y_b(t)$ signals.

3. Dynamics governing the time-varying NEC bifurcation

With the result presented in Fig. 5a, exploring the dynamics for the $Y_b(t)$ changes becomes equivalent to clarifying the causes responsible for the observed SSH signals in the key region of 12°–14°N and 127°–130°E. In the tropical Pacific Ocean, SSH variability (or equivalently the changes in the upper-ocean layer thickness) is induced predominantly by the time-varying surface wind forcing. Many past studies have shown that the wind-induced SSH variability can be quantified by the 1 ½-layer reduced-gravity model (e.g., Meyers 1979; Kessler 1990; Qiu and Joyce 1992; Capotondi and Alexander 2001; Capotondi et al. 2003). Under the long-wave approximation, the linear vorticity equation governing the 1 ½-layer reduced-gravity model is given by

$$\frac{\partial h'}{\partial t} - c_R \frac{\partial h'}{\partial x} = -\frac{g' \nabla \times \tau}{\rho_o g f} - \epsilon h', \tag{3}$$

where $h'(x, y, t)$ is the SSH anomaly, $c_R(x, y)$ is the speed of long baroclinic Rossby waves, g' is the reduced gravity, ρ_o is the reference density, $\boldsymbol{\tau}$ is the anomalous wind stress vector, and ϵ is the Newtonian dissipation rate. Given the

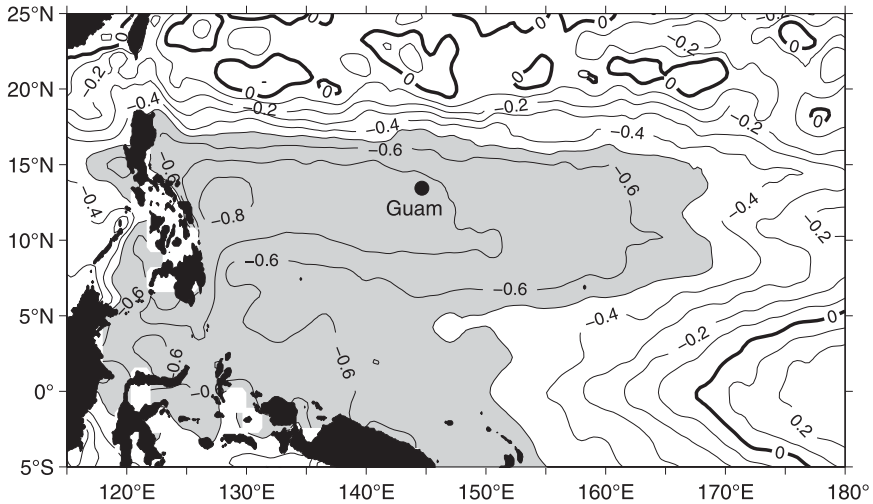

FIG. 4. Instantaneous linear correlation coefficient between the monthly time series of the NEC bifurcation $Y_b(t)$ and the SSH anomalies for the period of October 1992–December 2009. Areas where the correlation coefficient amplitude exceeds 0.5 are shaded. The black dot at 13.43°N, 144.65°E indicates the Guam tide gauge station.

observed wind stress curl data, $h'(x, y, t)$ can be solved by integrating Eq. (3) from the eastern boundary ($x = x_e$) along the baroclinic Rossby wave characteristic,

$$h'_m(x, y, t) = \frac{g'}{\rho_o g f} \int_{x_e}^{x} \frac{1}{c_R} \nabla \times \boldsymbol{\tau}\left(x', y, t + \frac{x - x'}{c_R}\right) \times \exp\left[\frac{\epsilon}{c_R}(x - x')\right] dx', \quad (4)$$

where h'_m signifies the SSH anomalies deduced from the wind-driven, 1 ½-layer reduced-gravity model. In Eq. (4), we have ignored the solution due to the eastern boundary forcing because its influence is limited to the area a few Rossby radii away from the boundary (see Fu and Qiu 2002). The confinement of the boundary-forced SSH signals can be visually confirmed in Fig. 6a, in which the SSH anomalies observed in the 12°–14°N band are plotted as a function of time and longitude.

Figure 6b shows the time–longitude plot of the modeled h'_m field in the 12°–14°N band with the use of $g' = 0.05$ m s^{-2}, $\epsilon = ½$ yr, and the monthly wind stress data from the European Center for Medium-Range Weather Forecasts (ECMWF) Ocean Analysis System ORA-S3 (Balmaseda et al. 2008). Both the g' and ϵ values are determined empirically by comparing modeled and observed SSH anomalies. The horizontal resolution of the ORA-S3 wind data is 1° × 1° and covers the period from January 1959 to December 2009. For the long baroclinic Rossby wave speed $c_R(x, y)$, we use the values derived by Chelton et al. (1998). In the 12°–14°N band, c_R has values ranging from 0.12 m s^{-1} in the eastern basin to 0.22 m s^{-1} in the western basin, and these values result in a basin transit time of ~2.6 yr. Compared to the observed SSH anomalies shown in Fig. 6a, the linear vorticity model captures well the large-scale SSH anomaly signals. For example, both the model and observations show the dominance of annual cycles of SSH anomalies in the central and eastern basins and that the interannual and longer time-scale variability prevails in the Philippine basin west of 160°E. The linear correlation between the observed and modeled h' fields in Fig. 6 has an overall coefficient $r = 0.74$, and this coefficient value is somewhat larger, $r = 0.88$, in the region that is key to the NEC bifurcation: 12°–14°N and 127°–130°E. Notice that smaller-scale SSH anomalies are also present in the observations (Fig. 6a) and these features are not reproduced by the linear vorticity dynamics of Eq. (3).

Following the same least squares fitting procedure that derives the proxy bifurcation latitude from the observed SSH anomaly data, we can infer the NEC's bifurcation latitude $Y_m(t)$ using the modeled SSH anomaly time series,

$$Y_m(t) = 11.9 - 0.17 \times h'_m(t) \quad (°\text{N}), \quad (5)$$

where $h'_m(t)$ is the monthly modeled SSH anomaly value (in cm) averaged in the 12°–14°N and 127°–130°E box. The gray line in Fig. 5b shows the monthly $Y_m(t)$ time series. Its low-pass filtered time series (the solid black line in Fig. 5b) has a predictive skill of $S = 85.0\%$ to the low-pass filtered $Y_b(t)$ signals. In other words, 85% of the variance of the low-frequency signals in Y_b can be

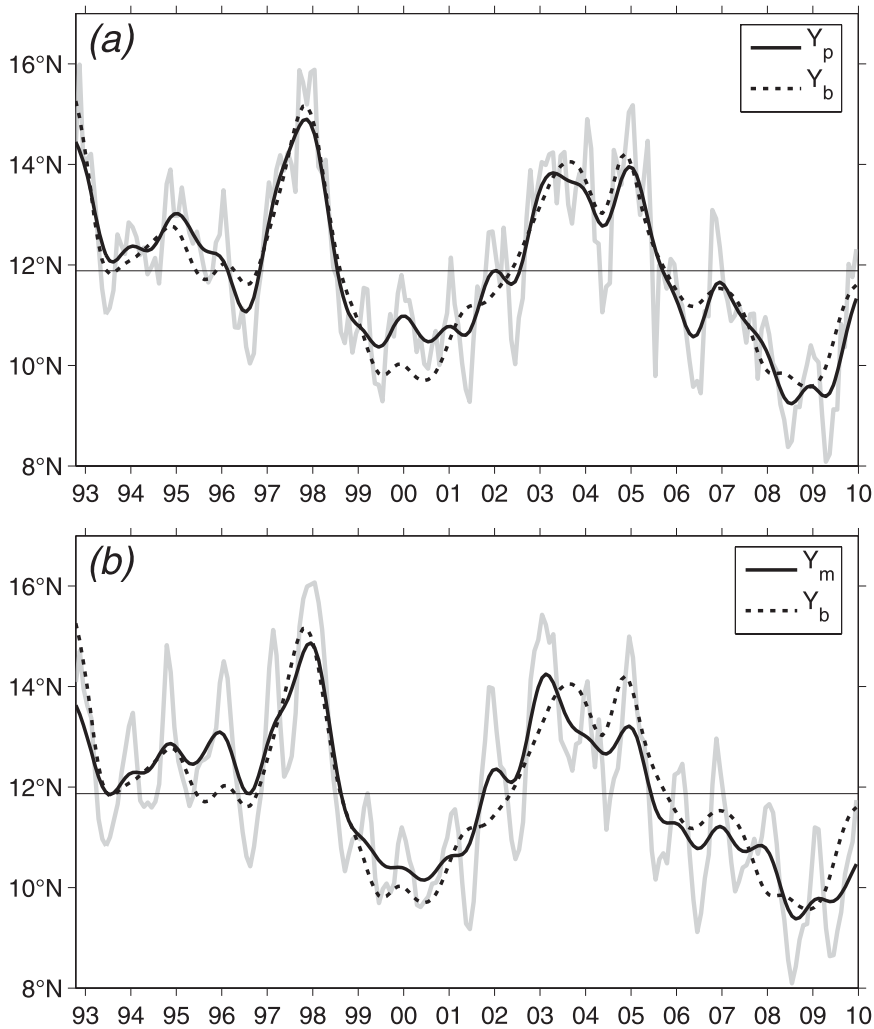

FIG. 5. (a) Time series of the proxy bifurcation latitude $Y_p(t)$ based on the observed SSH anomaly data in 12°–14°N and 127°–130°E [see Eq. (2)]. Gray and black lines denote the monthly and low-pass filtered $Y_p(t)$ time series, respectively. (b) As in (a), but for the model-inferred NEC bifurcation latitude $Y_m(t)$ based on Eq. (5). In (a) and (b), the dashed line denotes the observed, low-pass filtered $Y_b(t)$ time series.

accounted for by the SSH signals derived from the wind-driven 1 ½-layer reduced-gravity model.

4. Interannual-to-decadal changes in the NEC bifurcation

Although the variance of $Y_b(t)$ explained by the modeled SSH anomalies is not as high as that by the observed SSH signals (85.0% versus 92.3%), the linear vorticity model nevertheless provides us with a useful means to hindcast the NEC bifurcation latitude for the years before the era of satellite altimetry. With the ECMWF ORA-S3 wind stress data available from January 1959 and given the ~2.6-yr transit time by long baroclinic Rossby waves to cross the Pacific basin in the 12°–14°N band, we are able to extend the $h'_m(x, y, t)$ time series backward to January 1962.

Before examining the $Y_m(t)$ time series based on Eq. (5), it is desirable to verify the modeled, long-term SSH anomaly signals against independent observations. To achieve this, we utilize the tide gauge sea level data from Guam at 13.43°N and 144.65°E (see Fig. 4 for its location). Figure 7a compares the time series of the monthly SSH anomalies from the tide gauge measurement at Guam versus those of $h'_m(x, y, t)$ derived from Eq. (4) at the same location. An overall good correspondence between the two time series is easily discernible. Of particular relevance to the present study is that the correlation

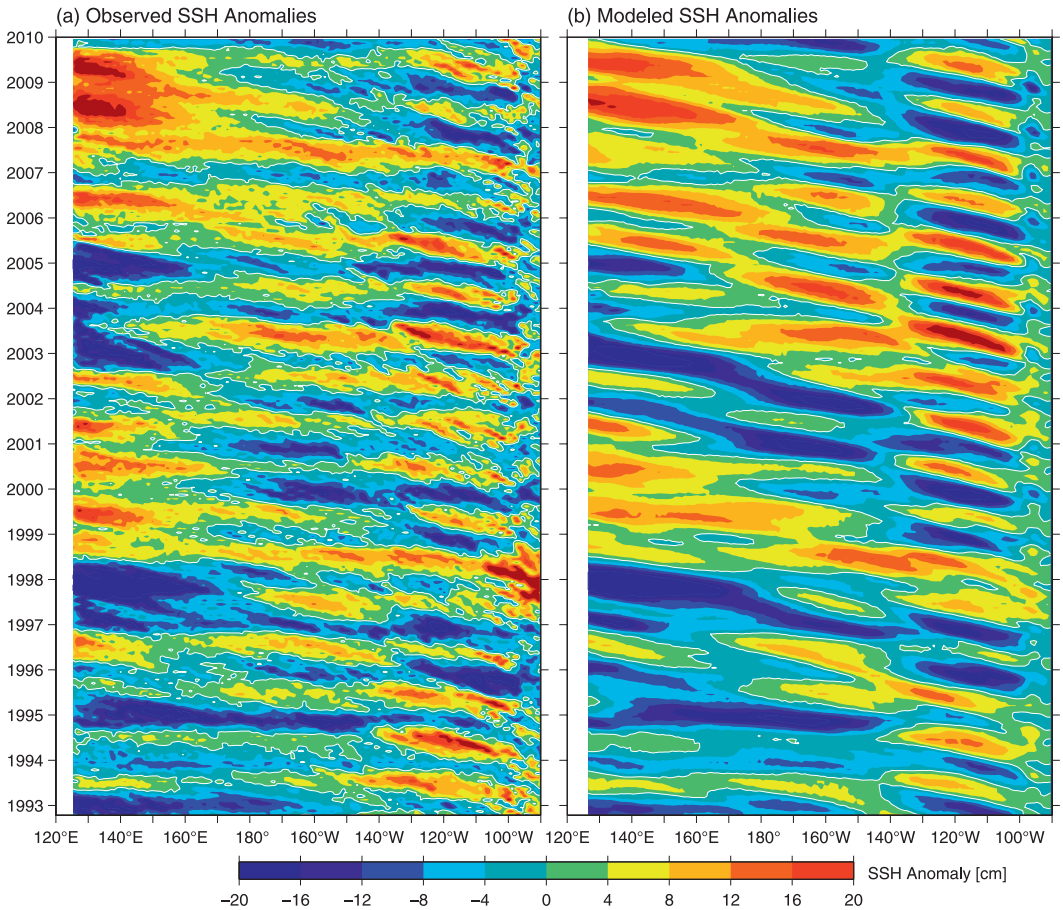

FIG. 6. (a) Time–longitude plot of the SSH anomalies in the 12°–14°N band from the satellite altimeter measurements. (b) As in (a), but from the wind-forced linear vorticity model of Eq. (4).

coefficients between the two time series have similar values (0.76 versus 0.86) for the periods before and after October 1992. This implies that there exist no biases in the wind forcing or model parameters between the periods before and after the altimetry era and that we could use the same statistical relationship of Eq. (5) to infer the NEC bifurcation latitude throughout the past half century.

Figure 7b shows the monthly $Y_m(t)$ and its low-pass filtered time series determined from Eq. (5). It is worth noticing that the quasi-decadal signals, which dominated the observed and modeled NEC bifurcation time series over the last 17 yr (Fig. 5), were insignificant in the years before 1992. As can be seen in Fig. 8a, based on the wavelet analysis, the NEC's bifurcation variability in the period of 1980–92 was dominated by signals with a wave period of 3–5 yr. Prior to 1970, Fig. 8a reveals that the $Y_m(t)$ variability had a weak spectral peak around 6 yr. During the 1970s, when the longer time-scale variance was low, it is interesting to note that there existed a compensating variance increase in the annual and biennial frequency bands in the $Y_m(t)$ variability.

Because the changes in $Y_m(t)$ reflect the cumulative effect of the time-varying wind forcing along the Rossby wave characteristics across the Pacific basin in the 12°–14°N band, it is important to quantify the relative contributions of the forcing along the different parts of the Pacific basin. One effective way to do so is to examine the cumulative $Y_m(t)$ variance explained by the wind forcing as a function of longitude X east of the key box of our interest,

$$S(X) \equiv 1 - \frac{\langle [\overline{h}'_m(x_e, t) - \overline{h}'_m(X, t)]^2 \rangle}{\langle \overline{h}'^2_m(x_e, t) \rangle}, \qquad (6)$$

where $\overline{h}'_m(X, t)$ denotes the box-averaged SSH anomaly value forced by the wind stress curl to the west of longitude X,

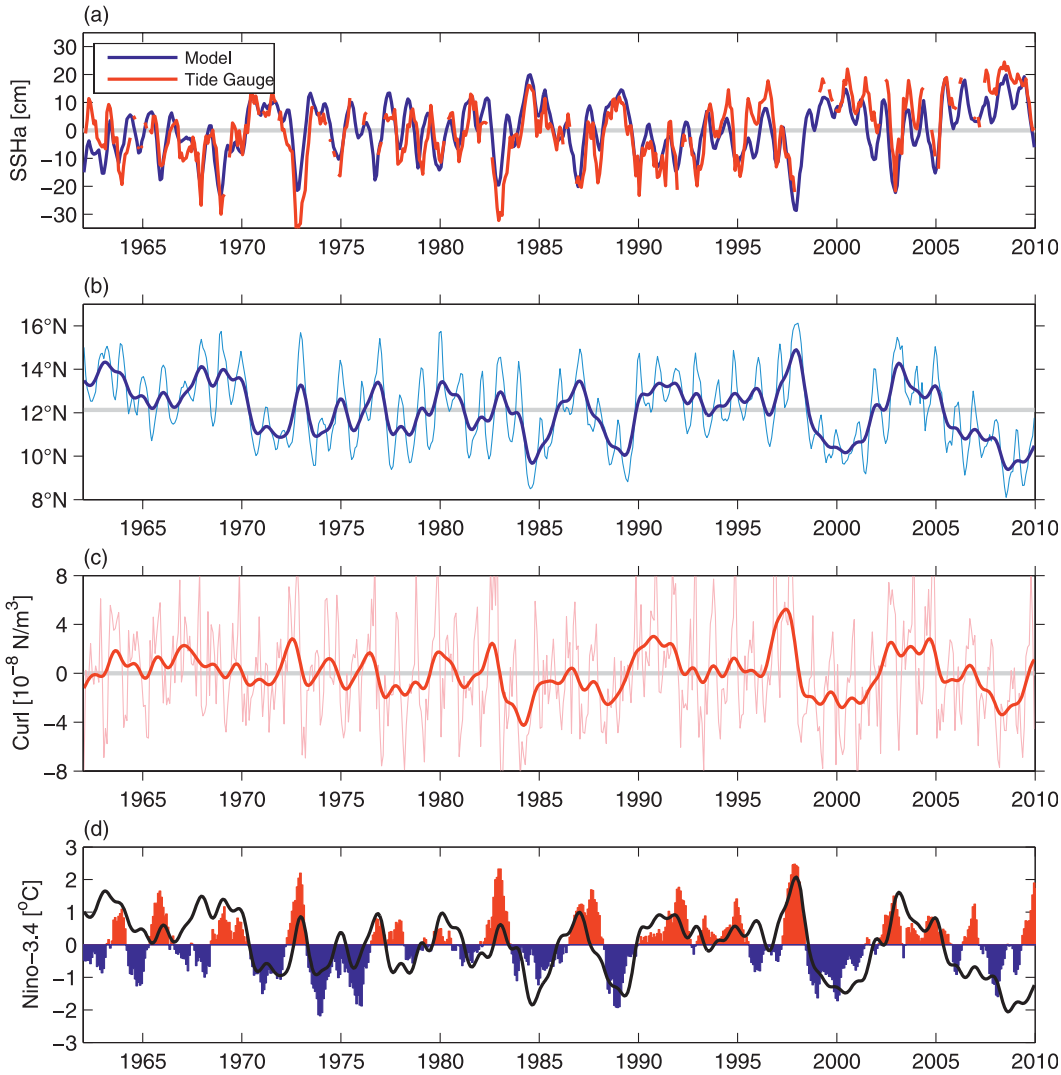

FIG. 7. (a) Time series of the SSH anomalies at Guam from the tide gauge measurements (red line) and the wind-forced linear vorticity model (blue line). (b) Time series of the model-inferred NEC bifurcation latitude $Y_m(t)$. (c) Time series of the wind stress curl anomalies averaged in 12°–14°N and 140°–170°E. In (b),(c), thin and thick lines denote the monthly and low-pass filtered time series, respectively. (d) Time series of the Niño-3.4 index (colored bars) and the low-pass filtered $Y_m(t)$. See (b) for the vertical scale of the $Y_m(t)$ time series.

$$\overline{h}'_m(X, t) = \frac{g'}{\rho_o g f L_x L_y} \int_{12^\circ\mathrm{N}}^{14^\circ\mathrm{N}} \int_{127^\circ\mathrm{E}}^{130^\circ\mathrm{E}} \left[\int_X^x \frac{1}{c_R} \nabla \times \boldsymbol{\tau}\left(x', y, t + \frac{x - x'}{c_R}\right) \exp \frac{\epsilon(x - x')}{c_R}\, dx' \right] dx\, dy, \tag{7}$$

and $L_x L_y$ denotes the area of the 12°–14°N and 127°–130°E box. By definition, $\overline{h}'_m(x_e, t)$ gives the same $h'_m(t)$ time series shown in Fig. 7b and $S(x_e) = 1$ in Eq. (6).

As shown in Fig. 9, the result of $S(X)$ reveals that much of the SSH variance in the key box off the NEC bifurcation is caused by the wind forcing in the western part of the Pacific basin: specifically, 80% of the SSH variation is induced by wind forcing to the west of the date line and the explained variance reaches 95% for the wind forcing west of 140°W. The dominance by the western basin forcing can be dynamically understood as follows. As indicated in Fig. 6, most of the wind-induced SSH anomalies east of 170°E have an annual frequency. Because it takes about 2 yr for the baroclinic Rossby waves in the 12°–14°N band to traverse from the eastern boundary to 170°E, these annually forced SSH signals

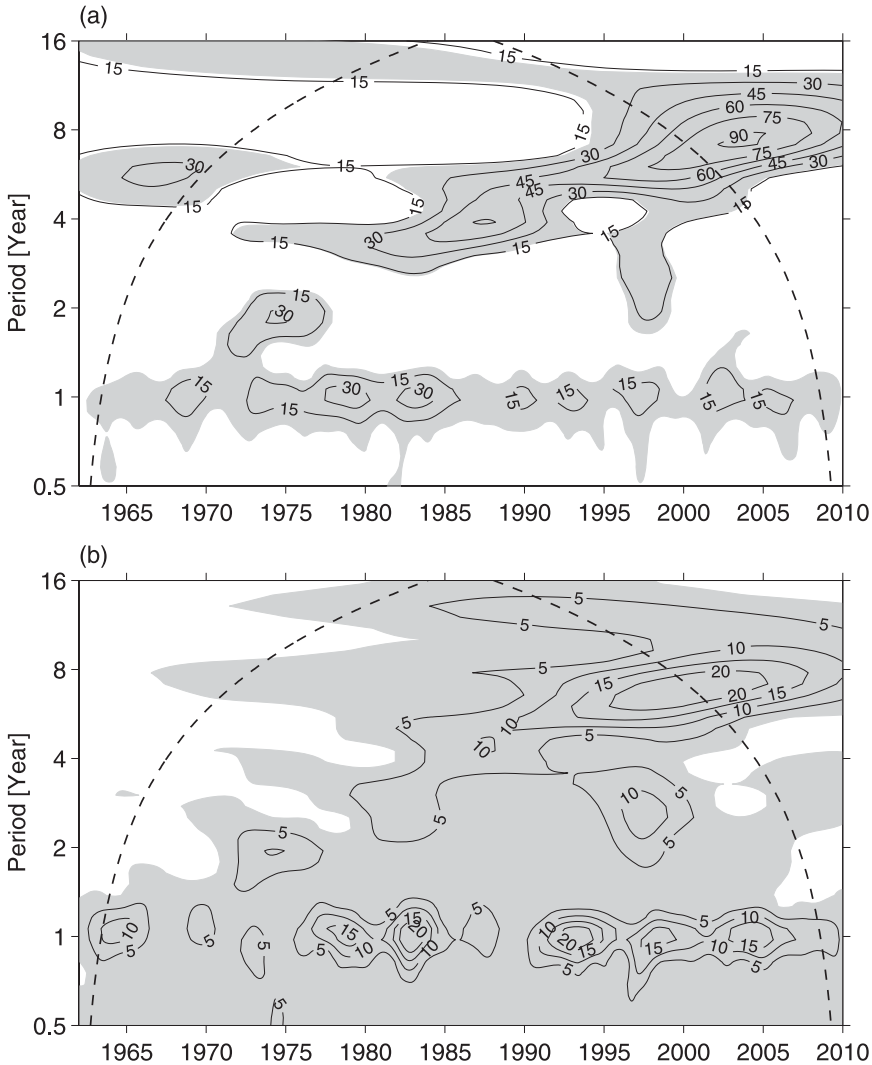

FIG. 8. (a) Wavelet power spectrum for the model-inferred NEC bifurcation latitude $Y_m(t)$. Contour unit in $(°)^2$. (b) As in (a), but for the wind stress curl anomalies averaged in 12°–14°N and 140°–170°E. Contour unit in 10^{-17} $(\mathrm{N\ m^{-3}})^2$. In (a) and (b), shadings indicate estimates of >95% confidence level and dashed lines indicate cones of influence by the edge effects.

are destructively canceled out along the Rossby wave characteristics and exert little impact upon the SSH signals near the western boundary. In contrast, the wind forcing in the west basin has lower frequencies; because it is closer to the western boundary, the forced SSH signals can reach the western boundary without the destructive cancellation.

Given the importance of wind forcing in the western basin, it is of interest to have a closer look at the regional wind stress curl signals. In Fig. 7c, we plot the time series of the wind stress curl anomalies averaged in the area of 12°–14°N and 140°–170°E. As indicated in Fig. 9, the wind forcing from this longitudinal band explains ~60% of the model-derived $Y_m(t)$ variance. As compared with the $Y_m(t)$ time series shown in Fig. 7b, there exists a favorable correspondence between the wind and $Y_m(t)$ time series on the interannual and longer time scales. Indeed, the linear correlation coefficient between the low-pass filtered time series shown in Figs. 7b,c reaches 0.8 when the wind forcing leads $Y_m(t)$ by 5 months (see dashed line in Fig. 10).[2] Here, the two time series are positively correlated, because a positive wind stress curl anomaly strengthens the tropical gyre and leads to a

[2] The 5-month lag here is the time needed for the wind-induced baroclinic Rossby waves to reach the SSH box at 127°–130°E from the forcing longitude, 140°–170°E.

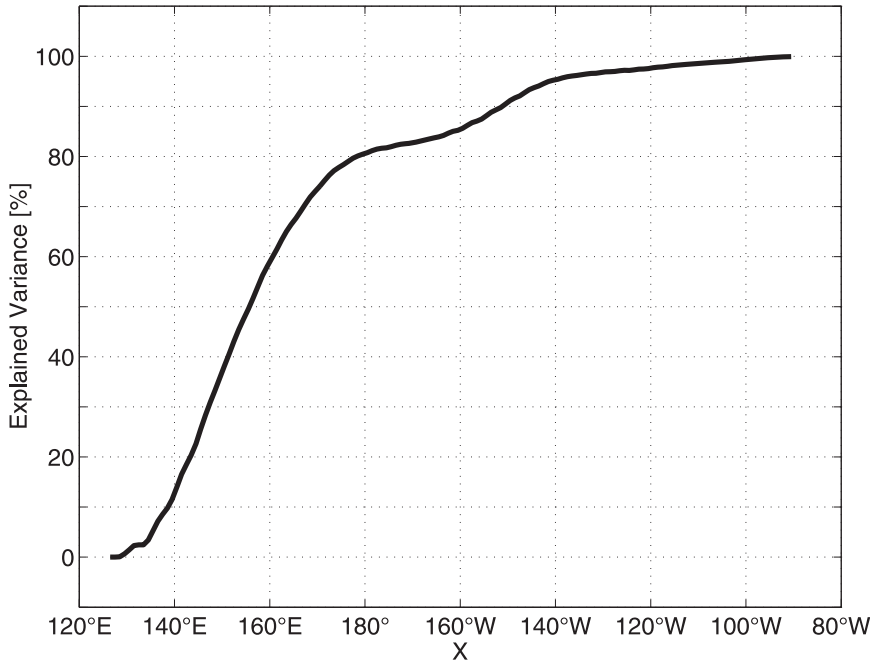

FIG. 9. Explained percent of variance of the model-inferred NEC bifurcation latitude $Y_m(t)$ by the cumulative wind forcing from 127°E to longitude X. See Eqs. (6) and (7) and the text for details.

northerly NEC bifurcation. As a consistency check, we plot in Fig. 8b the wavelet power spectrum for the wind stress curl time series shown in Fig. 7c. In agreement with the decadal modulations we noted for the $Y_m(t)$ time series, the low-frequency wind forcing had weak variance before 1970s, was dominated by signals in the ~(3–5)-yr band, and had predominantly quasi-decadal variance in the last two decades.

Several past studies have pointed out the connection between the low-frequency variation in the NEC bifurcation and the ENSO signals in the tropical Pacific Ocean (Qiu and Lukas 1996; Kim et al. 2004; Wang and Hu 2006). Because the lengths of the NEC bifurcation time series used in those studies were relatively short, and given the changes in characteristics of $Y_m(t)$ over time, it is important to reevaluate the ENSO connection based on the longer $Y_m(t)$ time series derived in this study. To represent the ENSO variability, we adopt in this study the Niño-3.4 index. Use of other ENSO indices, such as the Southern Oscillation index, does not alter qualitatively the conclusions reached below. Figure 7d shows the monthly Niño-3.4 index (in color) with the low-pass filtered $Y_m(t)$ time series superimposed. In accordance with the previous studies, there exists an overall good correspondence between the two time series: the NEC tends to bifurcate at a northerly latitude when the Niño-3.4 index is positive. A closer inspection of Fig. 7d, however, indicates that the amplitudes of the two time series do not match quite favorably. In fact, the linear correlation between the two time series is $r = 0.5$, indicating that the Niño-3.4 index explains only 25% of the $Y_m(t)$ variance (Fig. 10).

To further clarify the connection to ENSO, it is helpful to compare the surface wind forcing responsible for the $Y_m(t)$ signals with that associated with the ENSO variability. Figure 11a shows the surface wind stress vector and curl field regressed to the normalized, low-pass filtered wind stress curl anomaly time series in the 12°–14°N and 140°–170°E band (recall Fig. 7c). As we noted above, ~60% of the modeled $Y_m(t)$ variability is induced by the wind forcing from this band. On the broad spatial scales, this wind forcing is associated with a cyclonic atmospheric circulation over the entire western tropical Pacific Ocean. For comparison, the surface wind stress and curl field regressed to the normalized Niño-3.4 index is shown in Fig. 11b. Not surprisingly, the regressed wind signals have large amplitudes in the equatorial band. Along the 12°–14°N band important for the NEC bifurcation, the regressed positive wind stress curls are smaller in amplitude and are zonally less coherent than those shown in Fig. 11a. For example, the wind stress curl forcing west of 140°E is mostly uncorrelated to the ENSO variability. As we found in Fig. 9, the wind forcing west of 140°E can account for 15% of the time-varying $Y_m(t)$ variance. From the results of Fig. 11, we conclude that, although an ENSO index is able to serve as an indicator for the time-varying NEC

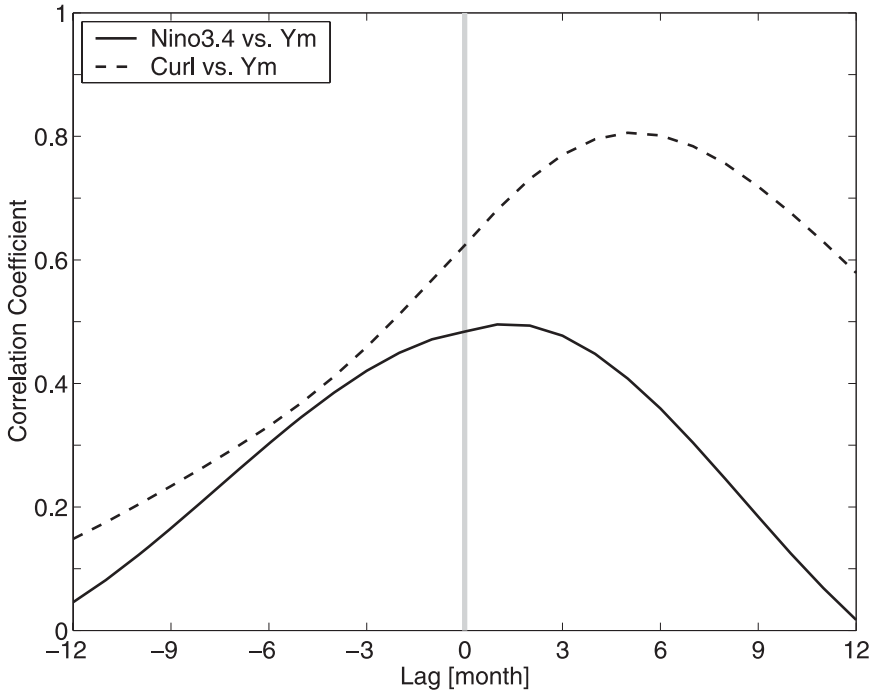

FIG. 10. The lagged correlation between the Niño-3.4 index and the low-pass filtered $Y_m(t)$ time series shown in Fig. 7d (solid line). Positive lags denote the lead of the Niño-3.4 index. The lagged correlation between the low-pass filtered wind stress curl anomalies and $Y_m(t)$ (dashed line). Positive lags denote the lead of the wind stress curl signals.

bifurcation on the interannual and longer time scales, the exact latitude of the NEC bifurcation is determined by the surface wind forcing in the 12°–14°N band in the western Pacific basin, whose signals are not fully represented by ENSO indices.

5. Summary

Sea surface height data from the multiple satellite altimeter missions of the past 17 yr are used to investigate the time-varying NEC bifurcation along the Philippine coast. The observed migration of the NEC bifurcation is large in amplitude and has a quasi-decadal frequency. The NEC bifurcated at a northerly latitude of ~14°N in late 1992, 1997–98, and 2003–04 and at a southerly latitude of ~10°N in 1999–2000 and 2007–09. When the NEC bifurcates at the northerly latitude, its surface transport tends to increase, the Kuroshio and Mindanao Current tend to intensify, and the SSH values tend to decrease in regions surrounding the Philippines and the Indonesian archipelagos. The reverse is true when the NEC bifurcation shifts to the south.

The time-varying NEC bifurcation signals can be approximated well by the SSH anomalies in the 12°–14°N and 127°–130°E box east of the mean NEC bifurcation point. The variance explained by the proxy SSH anomaly signals reach as high as 92% of the observed variance of the NEC bifurcation. The SSH anomaly signals in the 12°–14°N and 127°–130°E box can be adequately simulated using a 1 ½-layer reduced-gravity model forced by the ECMWF ORA-S3 reanalysis wind stress data. Use of the modeled SSH anomalies as a proxy accounts for 85% of the observed NEC bifurcation variance in the period of the last 17 yr.

With the confirmation of the modeled SSH anomaly signals serving well as a proxy, we extended the model-derived NEC bifurcation latitude time series back to 1962 based on the available ECMWF reanalysis wind stress data. A wavelet analysis reveals that the quasi-decadal changes in the NEC bifurcation became prominent only in the last 2 decades. During the 1980s, the NEC bifurcation was dominated by changes with a 3–5-yr period, and the NEC bifurcation had relatively low variance prior to 1970s. These interdecadal modulations in the characteristics of the NEC bifurcation reflect similar modulations in the characteristics of the surface wind forcing field over the past half century.

The surface wind forcing that is most relevant to the NEC bifurcation resides in the 12°–14°N and 140°–170°E band. To the east of 170°E, the wind stress curl forcing is

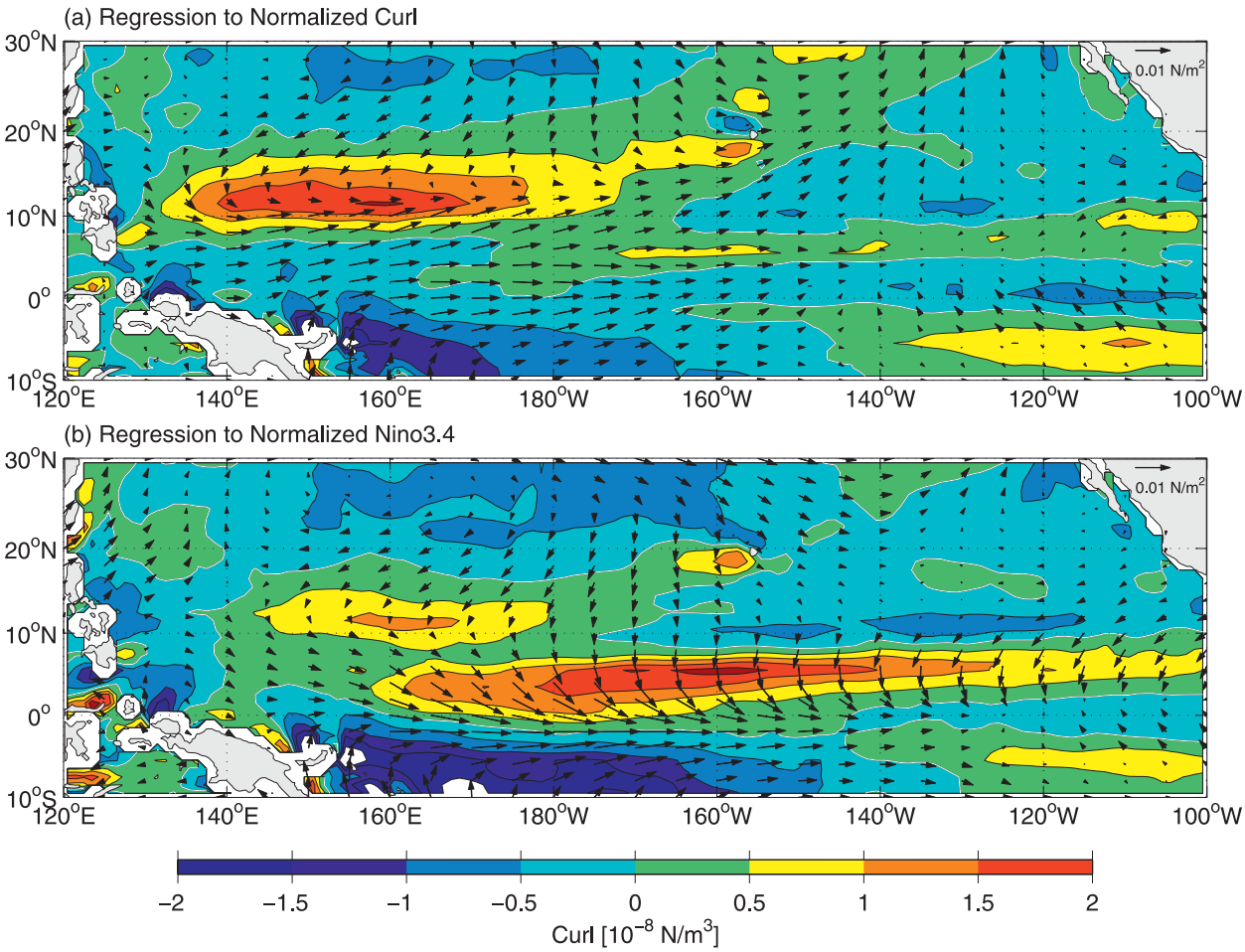

FIG. 11. (a) Wind stress vector and curl regressed to the normalized, low-pass filtered wind stress curl anomaly time series shown in Fig. 7c. (b) As in (a), but regressed to the normalized Niño-3.4 index shown in Fig. 7d.

dominated by annually varying signals. The annually forced SSH anomalies do not contribute effectively to the NEC bifurcation variability because they tend to cancel out as the signals propagate westward from the eastern boundary to 170°E over an approximately 2-yr journey. To the west of 170°E, the wind stress curl forcing has more variance in the interannual and longer frequency bands and the SSH signals induced there can directly impact the NEC bifurcation. Although a positive (negative) Niño-3.4 index can be utilized as a general indicator for a northerly (southerly) NEC bifurcation, the exact NEC bifurcation latitude depends on the surface wind forcing over the western tropical North Pacific Ocean containing variability not fully representable by the commonly used ENSO indices.

Acknowledgments. This study benefited from discussions with Luca Centurioni, Billy Kessler, Axel Timmermann, and Niklas Schneider. Detailed comments made by the anonymous reviewers helped improve an early version of the manuscript. We thank Magdelena Balmaseda and Jim Potemra for providing the ECMWF ORA-S3 surface wind stress data via the IPRC's Asia-Pacific Data Research Center. The merged satellite altimeter data were provided by the CLS Space Oceanography Division as part of the Environment and Climate EU ENACT project. This research was supported by Grant N00014-10-1-0267 of ONR and by Contract 1207881 from JPL as part of the NASA Ocean Surface Topography Mission.

REFERENCES

Amedo, C. L. A., C. L. Villanoy, and M. J. Udarbe-Walker, 2002: Indicators of upwelling at the northern Bicol shelf. *UPV J. Nat. Sci.,* **7,** 42–52.

Balmaseda, M. A., A. Vidard, and D. L. T. Anderson, 2008: The ECMWF Ocean Analysis System: ORA-S3. *Mon. Wea. Rev.,* **136,** 3018–3034.

Capotondi, A., and M. A. Alexander, 2001: Rossby waves in the tropical North Pacific and their role in decadal thermocline variability. *J. Phys. Oceanogr.,* **31,** 3496–3515.

——, ——, and C. Deser, 2003: Why are there Rossby wave maxima in the Pacific at 10°S and 13°N? *J. Phys. Oceanogr.,* **33,** 1549–1563.

Centurioni, L. R., P. P. Niiler, and D.-K. Lee, 2004: Observations of inflow of Philippine Sea water into the South China Sea through the Luzon Strait. *J. Phys. Oceanogr.,* **34,** 113–121.

Chelton, D. B., R. A. de Szoeke, M. G. Schlax, K. E. Naggar, and N. Siwertz, 1998: Geographical variability of the first baroclinic Rossby radius of deformation. *J. Phys. Oceanogr.,* **28,** 433–460.

Ducet, N., P.-Y. Le Traon, and G. Reverdin, 2000: Global high-resolution mapping of ocean circulation from TOPEX/Poseidon and ERS-1 and -2. *J. Geophys. Res.,* **105,** 19 477–19 498.

Fine, R. A., R. Lukas, F. M. Bingham, M. J. Warner, and R. H. Gammon, 1994: The western equatorial Pacific: A water mass crossroads. *J. Geophys. Res.,* **99,** 25 063–25 080.

Firing, E., Y. Kashino, and P. Hacker, 2005: Energetic subthermocline currents observed east of Mindanao. *Deep-Sea Res.,* **52,** 605–613.

Fu, L.-L., and B. Qiu, 2002: Low-frequency variability of the North Pacific Ocean: The roles of boundary- and wind-driven baroclinic Rossby waves. *J. Geophys. Res.,* **107,** 3220, doi:10.1029/2001JC001131.

Hu, D., and M. Cui, 1991: The western boundary current of the Pacific and its role in the climate. *Chin. J. Oceanol. Limnol.,* **9,** 1–14.

Kashino, Y., A. Ishida, and Y. Kuroda, 2005: Variability of the Mindanao Current: Mooring observation results. *Geophys. Res. Lett.,* **32,** L18611, doi:10.1029/2005GL023880.

——, N. Espana, F. Syamsudin, K. J. Richards, T. Jensen, P. Dutrieux, and A. Ishida, 2009: Observations of the North Equatorial Current, Mindanao Current, and the Kuroshio Current system during the 2006/07 El Niño and 2007/08 La Niña. *J. Oceanogr.,* **65,** 325–333.

Kessler, W. S., 1990: Observation of long Rossby waves in the northern tropical Pacific. *J. Geophys. Res.,* **95,** 5183–5217.

Kim, Y. Y., T. Qu, T. Jensen, T. Miyama, H. Mitsudera, H.-W. Kang, and A. Ishida, 2004: Seasonal and interannual variations of the North Equatorial Current bifurcation in a high-resolution OGCM. *J. Geophys. Res.,* **109,** C03040, doi:10.1029/2003JC002013.

Kimura, S., T. Inoue, and T. Sugimoto, 2001: Fluctuations in the distribution of low-salinity water in the North Equatorial Current and its effect on the larval transport of the Japanese eel. *Fish. Oceanogr.,* **10,** 51–60.

Le Provost, C., 2001: Ocean tides. *Satellite Altimetry and Earth Sciences,* L.-L. Fu and A. Cazenava, Eds., Academic Press, 267–303.

Le Traon, P.-Y., F. Nadal, and N. Ducet, 1998: An improved mapping method of multi-satellite altimeter data. *J. Atmos. Oceanic Technol.,* **25,** 522–534.

Locarnini, R. A., A. V. Mishonov, J. I. Antonov, T. P. Boyer, and H. E. Garcia, 2006: *Temperature*. Vol. 1, *World Ocean Atlas 2005,* NOAA Atlas NESDIS 61, 182 pp.

Lukas, R., E. Firing, P. Hacker, P. L. Richardson, C. A. Collins, R. Fine, and R. Gammon, 1991: Observations of the Mindanao Current during the Western Equatorial Pacific Ocean Circulation Study. *J. Geophys. Res.,* **96,** 7089–7104.

Meyers, G., 1979: On the annual Rossby wave in the tropical North Pacific Ocean. *J. Phys. Oceanogr.,* **9,** 663–674.

Nitani, H., 1972: Beginning of the Kuroshio. *Kuroshio: Its Physical Aspects,* H. Stommel and K. Yoshida, Eds., University of Tokyo Press, 129–163.

Qiu, B., and T. M. Joyce, 1992: Interannual variability in the mid- and low-latitude western North Pacific. *J. Phys. Oceanogr.,* **22,** 1062–1079.

——, and R. Lukas, 1996: Seasonal and interannual variability of the North Equatorial Current, the Mindanao Current and the Kuroshio along the Pacific western boundary. *J. Geophys. Res.,* **101,** 12 315–12 330.

——, M. Mao, and Y. Kashino, 1999: Intraseasonal variability in the Indo-Pacific Throughflow and the regions surrounding the Indonesian Seas. *J. Phys. Oceanogr.,* **29,** 1599–1618.

Qu, T., and R. Lukas, 2003: The bifurcation of the North Equatorial Current in the Pacific. *J. Phys. Oceanogr.,* **33,** 5–18.

Rio, M.-H., P. Schaeffer, G. Moreaux, J.-M. Lemoine, and E. Bronner, 2009: A new mean dynamic topography computed over the global ocean from GRACE data, altimetry and in-situ measurements. *Proc. OceanObs'09 Symp.,* Venice, Italy, IOC/UNESCO and ESA. [Available online at http://www.aviso.oceanobs.com/fileadmin/documents/data/products/auxiliary/MDT_Cnes-CLS09_poster_Oceanobs09.pdf.]

Toole, J., R. Millard, Z. Wang, and S. Pu, 1990: Observations of the Pacific North Equatorial Current bifurcation at the Philippine coast. *J. Phys. Oceanogr.,* **20,** 307–318.

Wang, Q., and D. Hu, 2006: Bifurcation of the North Equatorial Current derived from altimetry in the Pacific Ocean. *J. Hydrodyn.,* **18B,** 620–626.

Yaremchuk, M., and T. Qu, 2004: Seasonal variability of the large-scale currents near the Philippine coast. *J. Phys. Oceanogr.,* **34,** 844–855.